

# Optics Letters

## Two-dimensional photonic-crystal-based Fabry–Perot etalon

CHONG PEI HO,<sup>1,2</sup> PRAKASH PITCHAPPA,<sup>1,2</sup> PIOTR KROPELNICKI,<sup>3</sup> JIAN WANG,<sup>2</sup> HONG CAI,<sup>2</sup> YUANDONG GU,<sup>2</sup> AND CHENGKUO LEE<sup>1,\*</sup>

<sup>1</sup>Department of Electrical and Computer Engineering, National University of Singapore, 4 Engineering Drive 3, Singapore 117576, Singapore

<sup>2</sup>Institute of Microelectronics (IME), Agency for Science, Technology and Research (A\*STAR), 11 Science Park Road, Singapore 117685, Singapore

<sup>3</sup>Excelitas Technologies, 8 Tractor Road, Singapore 627969, Singapore

\*Corresponding author: [elelc@nus.edu.sg](mailto:elelc@nus.edu.sg)

Received 24 April 2015; revised 19 May 2015; accepted 19 May 2015; posted 21 May 2015 (Doc. ID 239745); published 5 June 2015

**We demonstrate the design, fabrication, and characterization of a polycrystalline-silicon-based photonic crystal Fabry–Perot etalon, which is aimed to work in the mid-infrared wavelengths. The highly reflective mirrors required in a Fabry–Perot etalon are realized by freestanding polycrystalline-silicon-based photonic crystal membranes with etched circular air holes. A peak reflection of 96.4% is observed at 3.60  $\mu\text{m}$ . We propose a monolithic CMOS-compatible fabrication process to configure two such photonic crystal mirrors to be in parallel to form a Fabry–Perot etalon; a filtered transmission centered at 3.51  $\mu\text{m}$  is observed. The quality factor measured is around 300, which is significantly higher than in existing works. This creates the possibility of using such devices for high-resolution applications such as gas sensing and hyperspectral imaging. © 2015 Optical Society of America**

**OCIS codes:** (230.5298) Photonic crystals; (050.2230) Fabry-Perot; (160.5293) Photonic bandgap materials; (310.6860) Thin films, optical properties.

<http://dx.doi.org/10.1364/OL.40.002743>

Optical reflectors play an important role in the realization of many optoelectronic devices and photonic elements such as mirrors, sensors, and interferometers. Due to its small size and excellent optical performance [1,2], photonic crystal (PhC)-based mirrors have proven to be an attractive design for a reflective mirror. In particular, 2D PhC has been shown to display extremely high reflection with only a single layer of dielectric [3–5]. With properly designed parameters, high reflection can practically be achieved across different frequency regions, including mid-infrared (MIR) regions.

By placing two such PhC mirrors in parallel to each other, a Fabry–Perot etalon (FPE) can be realized. With the inclusion of microelectromechanical systems (MEMS) technology, the gap between the mirrors can be tuned. The use of PhC mirrors also provides a much higher-quality ( $Q$ ) factor. In this work, we will

demonstrate the design, fabrication, and characterization of a freestanding PhC-based mirror. Subsequently, the PhC-based mirrors are used in the FPE, which is fabricated using a CMOS-compatible monolithic fabrication process that is highly desirable [6]. This is in contrast to existing works that typically involve bonding of the mirrors or the use of non-CMOS compatible materials such as polyimide as sacrificial material to define the cavity length [7–11]. In our previous works [12,13], where we fabricated only the PhC mirror, the process used involved a high-temperature anneal of 1000°C. Such an approach is not adopted in this Letter due to the increase in the number of polycrystalline silicon (Si) and silicon dioxide ( $\text{SiO}_2$ ) layers in the FPE. The annealing step induces very high thermal stress, which causes cracking of the silicon layers and wafer breakage. In this Letter, we will alleviate this issue through the use of low-stress epitaxial polycrystalline Si, which is deposited at a lower temperature of 610°C. The fabricated FPE shows a transmission peak centered at 3.51  $\mu\text{m}$  with a  $Q$  factor of around 300. While this is lower than simulations, it is still significantly higher than in existing works, which typically have a  $Q$  factor of a few tens [8–10]. This opens the possibility of utilizing such PhC FPE for high-resolution applications like gas sensing [14,15] and hyperspectral imaging [7,8].

The PhC mirror is defined by having circular air holes etched from polycrystalline Si slab. The band structure of the PhC structure can be calculated based on plane wave expansion method, as shown in Fig. 1.

The frequency of the bandgap (shaded in red) corresponds to the wavelength region where high reflection is expected. Based on the designed parameters of  $r/a$  and  $t/a$  being 0.395 and 0.513, respectively, where  $r$  is the radius of the air hole,  $t$  is the thickness of the Si slab, and  $a$  is the periodicity, the bandgap is from 0.528 ( $2\pi/a$ ) to 0.586 ( $2\pi/a$ ). When the periodicity is set to be 1.95  $\mu\text{m}$ , the wavelength region of high reflection is from 3.33 to 3.69  $\mu\text{m}$ . Optimization of the parameters is then performed through the use of commercially available software from Lumerical Solutions Inc. [16], which is based on the three-dimensional (3-D) finite difference time domain (FDTD) method. The unit cell consists of the Si slab with

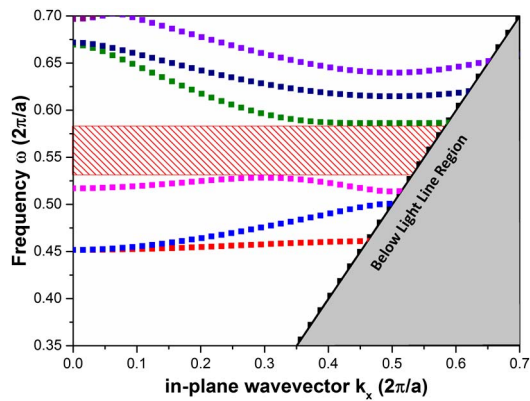


Fig. 1. Band structure of the PhC mirror.

a length of  $1.95 \mu\text{m}$ , and the refractive index of Si is set to  $3.464$ . A cylinder of air hole with a height similar to the Si slab is then defined concentrically. The boundary conditions at the sides of the unit cell are set to a periodic boundary condition, and perfectly matched layers are included to prevent unwanted reflection off the simulation boundaries. When the air hole radius and the Si slab thickness are fixed at  $0.77 \mu\text{m}$  and  $1 \mu\text{m}$ , the maximum simulated reflection is at  $3.60 \mu\text{m}$ .

The PhC mirror is suspended in order to make it compatible with subsequent fabrication of the FPE and also to enhance its performance by reducing leakage through the underlying  $\text{SiO}_2$ . The schematic of the device is shown in Fig. 2(a). Fabrication of the PhC mirror starts by growing a  $1 \mu\text{m}$  thermal  $\text{SiO}_2$  on a bare 8-in. Si wafer. The device layer of  $1 \mu\text{m}$  thick polycrystalline Si is then deposited by using epitaxy. The air holes are patterned using deep UV lithography and etched using deep reactive ion etching (DRIE). DRIE is then used to etch the Si substrate, and the whole PhC mirror is released using vapor hydrofluoric acid (VHF). The scanning electron microscope (SEM) of the fabricated PhC membrane is shown in Fig. 2(b), and it is found that the fabricated parameters are highly matched with the designed parameters. Measurement of the PhC mirror is done using an Agilent Cary 620 FTIR microscope from  $2$  to  $8 \mu\text{m}$ . Due to the experimental setup, the angle of incidence for the reflection measurement is limited to  $45^\circ$ . As the subsequent measurement of the FPE is based on transmission, which has an angle of incidence fixed to normal incidence, the dependence of the performance of the PhC mirror with incident angle is investigated. Based on 3D FDTD simulations of the PhC mirror, the wavelength of high reflection when the input IR light is incidence at  $45^\circ$  and normal incidence remains the same at  $3.60 \mu\text{m}$ . The size of the PhC mirror membrane is designed to be  $200 \mu\text{m} \times 200 \mu\text{m}$ , while the spot size of the

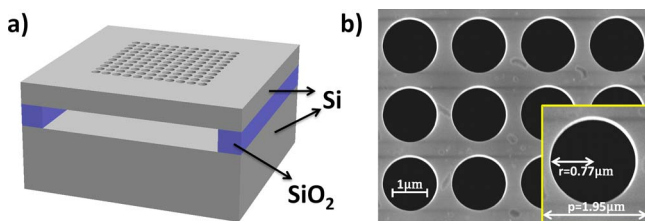


Fig. 2. (a) Schematic of PhC mirror. (b) SEM of fabricated chip.

MIR input is set to be  $100 \mu\text{m} \times 100 \mu\text{m}$  in order to ensure that the input beam is illuminated only on the PhC patterns. The reflection measurement of the PhC mirror is shown in Fig. 3. A high reflection of  $96.4\%$  is measured at  $3.60 \mu\text{m}$  with a bandwidth of  $160 \text{ nm}$  for wavelengths that have reflection of more than  $90\%$ . The dips in reflection observed at  $3.29$  and  $3.43 \mu\text{m}$  were looked into in our previous work [13], where we attributed them to the  $45^\circ$  angle of incidence.

The work is extended to form a PhC FPE, as mentioned above. This is done by placing two PhC mirrors in parallel with each other. We propose a monolithic approach to the fabrication process in order to avoid any physical bonding of the mirrors, which is usually used in existing works. Such a monolithic fabrication approach provides simplicity and low-risk fabrication, which can be achieved across the whole wafer. Based on the measurement results from the PhC mirror where the peak reflection is at  $3.60 \mu\text{m}$ , the cavity gap between the mirrors is designed to be around  $1.80 \mu\text{m}$ , which is half of the peak reflection wavelength. The schematic of the PhC FPE is shown in Fig. 4(a).

Fabrication of the FPE starts with a  $1 \mu\text{m}$  PECVD  $\text{SiO}_2$  on a bare Si wafer, as shown in Fig. 5(a). The device layer of  $1 \mu\text{m}$  thick polycrystalline Si of the bottom PhC mirror is then deposited using epitaxy [Fig. 5(b)]. Photolithography followed by DRIE of the polycrystalline Si layer to form the air holes is then performed to define the bottom PhC mirror [Fig. 5(c)]. A  $2 \mu\text{m}$  PECVD  $\text{SiO}_2$  is deposited [Fig. 5(d)] before chemical mechanical polishing (CMP) of  $0.2 \mu\text{m}$  of  $\text{SiO}_2$  is done to remove topology issues and also to define the cavity length of the

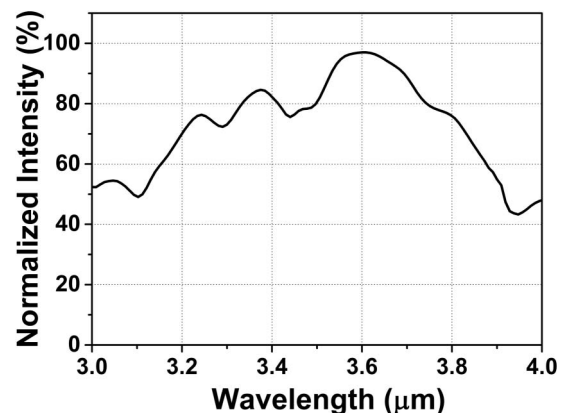


Fig. 3. Reflection measurement of the fabricated PhC mirror.

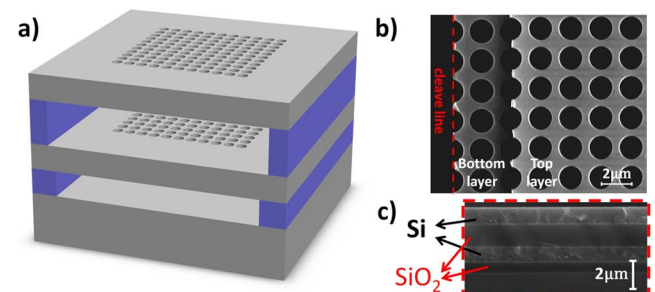


Fig. 4. (a) Schematic of PhC FPE, SEM of the (b) top and (c) cross-sectional view of the fabricated FPE before VHF release.

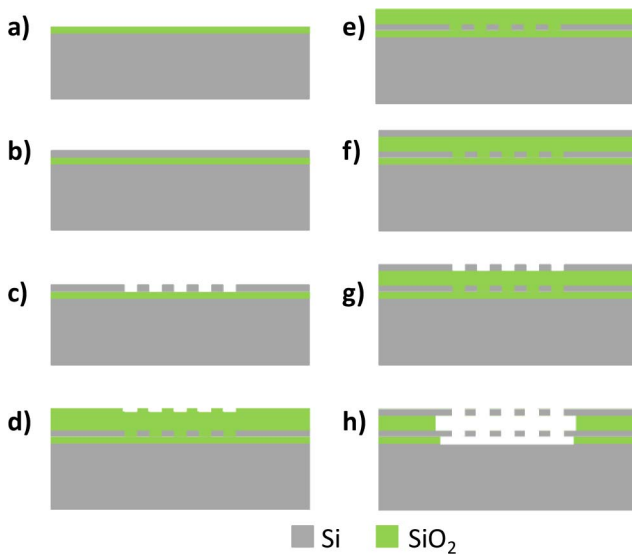


Fig. 5. Fabrication process of the FPE.

FPE [Fig. 5(e)]. The 1  $\mu\text{m}$  Si device layer of the top PhC mirror is then deposited using epitaxy [Fig. 5(f)], and the air holes are defined through photolithography and DRIE [Fig. 5(g)]. Finally, the FPE is released by using VHF [Fig. 5(h)]. The fabricated device is shown in Fig. 4(b). The device is cleaved in order to reveal the bottom PhC mirror. The cross-sectional view of the FPE before release is shown in Fig. 4(c). Due to thickness variation by the CMP process, the cavity length is measured to be only 1.70  $\mu\text{m}$ .

Simulation of the FPE is done using 3D FDTD as well, where two identical 1  $\mu\text{m}$  thick Si slabs with an air hole radius of 0.77  $\mu\text{m}$  are drawn with a separation defined by the cavity length. Similar to the PhC mirror simulation, the unit cell consists of the Si slabs with a length of 1.95  $\mu\text{m}$  on each side, and the refractive index of Si is set to 3.464. The boundary conditions are also set to periodic boundary conditions with perfectly matched layers. In order to obtain the theoretical  $Q$  factor of the FPE, unlike the PhC mirror, the expected high  $Q$  factor is determined by the slope of the envelope of the decaying signal in the simulation. This is because the energy within the cavity cannot completely decay in a time that can be simulated reasonably, and the maximum  $Q$  factor that can be simulated scales with the simulation time. The simulated  $Q$  factor in an optimized case of a cavity length of 1.80  $\mu\text{m}$  is found to be in excess of 45,000 at a wavelength of 3.59  $\mu\text{m}$  (ideal case), as shown in Fig. 6. However, after taking fabrication variations into account, the simulated  $Q$  factor drops to around 540 at 3.52  $\mu\text{m}$  (nonideal case). The enhanced  $Q$  factor over existing works is attributed to the additional filtering effects of the PhC mirror. The first filtering effect is within the Fabry–Perot cavity, where the undesired wavelengths are attenuated due to destructive interference. The second filtering effect is due to the intrinsic wavelength selective reflectivity of the PhC mirror, which has a bandwidth of around 160 nm and more than 90% reflection. In contrast, a multilayer Bragg reflector has a bandwidth of more than 3  $\mu\text{m}$  in the MIR wavelengths for reflection of more than 90% [17–19]. This makes the PhC mirror able to filter

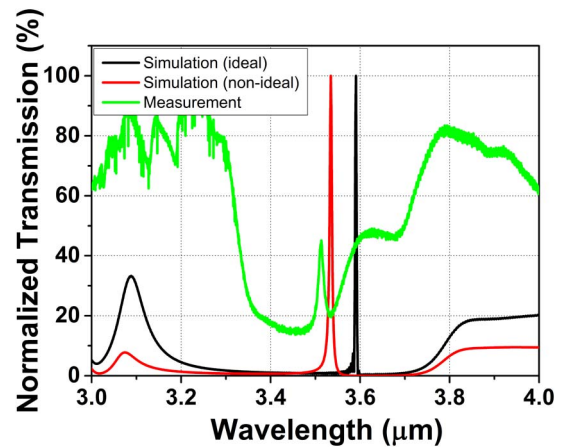


Fig. 6. Simulation of ideal and nonideal case of the FPE and measurement of the fabricated FPE.

unwanted wavelengths more efficiently than the multilayer Bragg reflector, hence resulting in a higher  $Q$  factor.

Measurement of the FPE is also done by an Agilent Cary 620 FTIR microscope from 2 to 8  $\mu\text{m}$ . Similarly, the size of the FPE is designed to be 200  $\mu\text{m}$   $\times$  200  $\mu\text{m}$ . In the case of transmission measurement, the incidence angle is normal to the sample. The measurement result is also shown in Fig. 6. Measurement of the fabricated device reveals a  $Q$  factor of around 300 at a wavelength of 3.51  $\mu\text{m}$ . The lower transmission intensity for a wavelength range below 3.35  $\mu\text{m}$  and above 3.55  $\mu\text{m}$  in the simulations can be attributed to the simulation methods adopted for the high  $Q$ -factor simulations, as the transmission intensity of wavelengths, where there are no resonances, are suppressed. While the measured  $Q$  factor is lower than the simulated  $Q$  factor, it is still around an order of magnitude higher than existing works where the  $Q$  factor is typically a few tens. The shift in the transmission wavelength and the drop in  $Q$  factor can be attributed to the variation in the cavity length. When the cavity length is not at the optimal distance, the MIR light is unable to be confined within the cavity due to higher transmission. This reduces the efficiency of the constructive interference of the desired wavelength, which causes a drop in output intensity as well as broadening of the transmission peak. Both of these factors result in a much lower  $Q$  factor. In addition, the presence of the Si substrate in the FPE causes a drop in the transmitted intensity. Based on measurement of bare Si, the transmitted intensity is reduced to around 60% for wavelengths around 3.60  $\mu\text{m}$ . The effect of the Si substrate will be removed in future iterations by performing a DRIE etch of the Si substrate. In order to alleviate the fabrication variations introduced by the CMP process on the cavity length, MEMS technology can be incorporated in the design. With MEMS technology, it will enable actuation of the PhC mirrors and, hence, achieve tunability of the cavity length. This not only reduces the impact of cavity length variation in fabrication process, it also offers the possibility of realizing a tunable Fabry–Perot interferometer.

In conclusion, we have demonstrated the development of polycrystalline-silicon-based PhC mirror and extended the work to realize a PhC FPE aiming to work in the mid-infrared wavelengths. The highly reflective PhC mirrors are realized

by fabricating freestanding polycrystalline Si membranes with etched circular air holes. We have proposed a monolithic approach in the fabrication in order to achieve simplicity and low risk. We observed a peak reflection of 96.4% at 3.60  $\mu\text{m}$  through measurement. We have also fabricated and characterized a PhC FPE based on knowledge obtained from the PhC mirror. With a high reflection at 3.60  $\mu\text{m}$ , the cavity length of the cavity is designed to be around 1.80  $\mu\text{m}$ . From simulations, the  $Q$  factor in an ideal scenario, where the optimized cavity length is 1.80  $\mu\text{m}$ , is found to be in excess of 45,000. After taking fabrication variations into account, the simulated  $Q$  factor is around 540. Measurement of the fabricated device reveals a  $Q$  factor of around 300, which is around an order of magnitude higher than in existing works. Coupled with MEMS technology to help achieve tunability and also to alleviate fabrication variations, this work offers great possibility of utilizing such PhC FPE for high-resolution applications such as gas sensing and hyperspectral imaging.

Ministry of Education–Singapore (MOE) (MOE2012-T2-2-154).

This work was supported by MOE2012-T2-245 2-154 (Monolithic Integrated Si/AlN Nanophotonics Platform for Optical NEMS and OEICs) from the Ministry of Education–Singapore (MOE) under WBS No. R-263-000-A59-112.

## REFERENCES

1. C. P. Ho, B. Li, A. J. Danner, and C. Lee, *Microsyst. Technol.* **19**, 53 (2013).
2. B. Li, C. P. Ho, F. L. Hsiao, and C. Lee, *J. Nanophoton.* **8**, 084090 (2014).
3. W. Zhou, D. Zhao, Y. Shuai, H. Yang, S. Chuwongin, A. Chadha, J.-H. Seo, K. Wang, V. Liu, Z. Ma, and S. Fan, *Prog. Quantum. Electron.* **38**, 1 (2014).
4. S. Fan and J. D. Joannopoulos, *Phys. Rev. B* **65**, 23 (2002).
5. C. P. Ho, P. Pitchappa, B. W. Soon, and C. Lee, *Opt. Express* **23**, 10598 (2015).
6. X. Wu, C. Jan, and O. Solgaard, *J. Microelectromech. Syst.* (to be published), doi: 10.1109/JMEMS.2014.2360859
7. A. J. Keating, J. Antoszewski, K. K. M. B. D. Silva, K. J. Winchester, T. Nguyen, J. M. Dell, C. A. Musca, L. Faraone, P. Mitra, J. D. Beck, M. R. Skokan, and J. E. Robinson, *J. Electron. Mater.* **37**, 1811 (2008).
8. T. J. Russin, M. Kerber, A. Russin, A. Wang, and R. Waters, *J. Microelectromech. Syst.* **21**, 181 (2012).
9. J. Mayrwöger, C. Mitterer, W. Reichl, C. Krutzler, and B. Jakoby, *Proc. SPIE* **8066**, 80660K (2011).
10. J. S. Milne, J. M. Dell, A. J. Keating, and L. Faraone, *J. Microelectromech. Syst.* **18**, 905 (2009).
11. C. A. Musca, J. Antoszewski, K. J. Winchester, A. J. Keating, T. Nguyen, K. K. M. B. D. Silva, J. M. Dell, L. Faraone, P. Mitra, J. D. Beck, M. R. Skokan, and J. E. Robinson, *IEEE Electron Dev. Lett.* **26**, 12 (2005).
12. C. P. Ho, P. Pitchappa, P. Kropelnicki, J. Wang, Y. Gu, and C. Lee, *IEEE J. Sel. Top. Quantum Electron.* **20**, C4 (2014).
13. C. P. Ho, P. Pitchappa, P. Kropelnicki, J. Wang, Y. Gu, and C. Lee, *J. Nanophoton.* **8**, 084096 (2014).
14. M. Noro, K. Suzuki, N. Kishi, H. Hara, T. Watanabe, and H. Iwaoka, *IEEE Sixteenth Annual International Conference on Micro Electro Mechanical Systems* (IEEE, 2003), p 319.
15. J. Wöllenstein, A. Eberhardt, S. Rademacher, and K. Schmitt, *Proc. SPIE* **8066**, 80660Q (2011).
16. FDTD Solutions, Lumerical Solutions, Vancouver, British Columbia, Canada 2013, <http://www.lumerical.com/tcad-products/fdtd>
17. M. Ebermann, N. Neumann, K. Hiller, M. Seifert, M. Meinig, and S. Kurth, *Proc. SPIE* **8977**, 89770T (2014).
18. M. Tuohiniemi and M. Blomberg, *J. Micromech. Microeng.* **21**, 075014 (2011).
19. Y. Shuai, D. Zhao, G. Medhi, R. Peale, Z. Ma, W. Buchwald, R. Soref, and W. D. Zhou, *IEEE Photon. J.* **5**, 1 (2013).